Coordinated multivesicular release at a mammalian ribbon synapse

Joshua H Singer[1], Luisa Lassová[2], Noga Vardi[2] & Jeffrey S Diamond[1]

Traditional models of synaptic transmission hold that release sites within an active zone operate independently. Although the release of multiple vesicles (multivesicular release; MVR) from single active zones occurs at some central synapses, MVR is not thought to require coordination among release sites. Ribbon synapses seem to be optimized to release many vesicles over an extended period, but the dynamics of MVR at ribbon synapses is unknown. We examined MVR at a ribbon synapse in a retinal slice preparation using paired recordings from presynaptic rod bipolar and postsynaptic AII amacrine cells. When evoked release was highly desynchronized, discrete postsynaptic events were larger than quantal miniature excitatory postsynaptic currents (mEPSCs) but had the same time course. The amplitude of these multiquantal mEPSCs, which seem to arise from the essentially simultaneous release of multiple vesicles, was reduced by lowering release probability. The release synchrony reflected in these multivesicular events suggests that release within an active zone is coordinated during MVR.

The quantal content (m) of an evoked response at the neuromuscular junction (NMJ) is closely matched to the number of anatomically defined presynaptic active zones[1], and vesicle release at the NMJ obeys Poisson statistics[2]. These facts, together with corroborating physiological evidence from other synapses, gave rise to the hypothesis that an active zone releases only one synaptic vesicle per presynaptic action potential, despite containing multiple release sites with docked vesicles[3,4]. Although a mechanism preventing the release of multiple vesicles from the same active zone has not been described, the very low release probability (P_R) at NMJ active zones would make MVR at these synapses very rare. In the central nervous system, however, where P_R generally is higher[5,6], MVR has been demonstrated at several synapses[7–10]. If multiple vesicles increase activation of postsynaptic receptors[9,10], MVR could enhance the information capacity of a synapse.

It is possible that MVR does not violate the tenet that individual release sites within an active zone operate independently[2]. MVR at inhibitory cerebellar synapses occurs with the same degree of asynchrony as evoked release[8], suggesting that the activity of individual release sites need not be coordinated to achieve MVR. Rather, MVR may be a direct consequence of high P_R (ref. 9)—a statistical side effect of increased reliability—though high P_R does not guarantee MVR[11].

Excitatory presynaptic terminals in the vertebrate retina are distinguished by a protein structure, the ribbon, to which synaptic vesicles are tethered. Though the ribbon's precise role is uncertain, the remarkable capacity of these synapses for exocytosis (*e.g.*, goldfish Mb1 bipolar cell terminals contain 45–65 ribbons[12] and can release 2,000–3,000 vesicles per second, which is ~50 vesicles per ribbon per second)[13,14] suggests that the ribbon organizes vesicles at release sites in a manner that facilitates MVR[15]. The dynamics of MVR from a single ribbon, however, has not been observed. Moreover, release from mammalian bipolar cell terminals, which contain fewer ribbons and vesicles than goldfish terminals, has not been characterized as thoroughly as in goldfish[16,17].

We examined transmission at glutamate-releasing ribbon synapses in the rat retina by making paired recordings from presynaptic rod bipolar cells (RBCs) and postsynaptic AII amacrine cells in acute retinal slices. Two experimental observations of evoked, relatively synchronous EPSCs supported MVR: first, glutamate concentration in the cleft during the EPSC varied with release probability, analogous to other descriptions of MVR[7,9,18]; second, m greatly exceeded the probable number of active zones at the synaptic contacts between the neurons. Under conditions favoring desynchronized release, evoked responses comprised distinct, multivesicular events reflecting almost perfectly simultaneous release: individual events were larger than spontaneous mEPSCs, though the time courses of the two were nearly indistinguishable, and their amplitudes varied with changes in P_R. We conclude that evoked exocytosis at ribbon synapses reflects coordination of multiple release sites within the same active zone.

RESULTS

Ca^{2+} tail currents elicit fast EPSCs

Voltage-clamp recordings were made from RBCs and AIIs in rat retinal slices[19]. RBC terminals receive glycinergic input[20] and γ-aminobutyric acid (GABA)-mediated inhibition via GABA$_A$ and GABA$_C$ receptors[19,21] (rat RBC terminals lack GABA$_B$ receptors[22]). Therefore, in the superfusate, we included tetrodotoxin (TTX), strychnine, picrotoxin and (1,2,5,6,-tetrahydropyridine)-methylphosphinic acid (TPMPA) to block voltage-gated Na$^+$ channels, glycine, GABA$_A$ and GABA$_C$ receptors, respectively (see Methods). This way, we were able to isolate

[1]Synaptic Physiology Unit, NIH/NINDS, 36 Convent Drive, MSC-4066, Building 36 Room 2C-09, Bethesda, Maryland 20892, USA. [2]Department of Neuroscience, University of Pennsylvania, 123 Anatomy/Chemistry Building, Philadelphia, Pennsylvania 19104-6058, USA. Correspondence should be addressed to J.H.S. (singerj@ninds.nih.gov).

EPSCs mediated by alpha-amino-3-hydroxy-5-methyl-4-isoxazole propionic acid (AMPA) receptors (AMPARs)[19].

Presynaptic Ca^{2+} tail currents following 10-ms steps from 60 to +90 mV elicited fast EPSCs (tEPSCs) in the AII (ref. 19; **Fig. 1a**). RBC-AII synapses showed substantial paired-pulse depression (PPD): a second tEPSC (100 ms interval) was $39 \pm 5\%$ as large as the first ($n = 6$; **Fig. 1a**). PPD appeared to be presynaptic: the paired-pulse ratio (PPR = $tEPSC_2/tEPSC_1$) increased from 0.39 ± 0.05 to 0.61 ± 0.04 ($n = 6$, $P = 0.005$; **Fig. 1a**) when we lowered extracellular $[Ca^{2+}]$ from 2.5 to 0.5 mM, thereby lowering P_R. In addition, the PPR (25 ms interval) was unchanged when postsynaptic AMPAR desensitization was blocked with cyclothiazide (CTZ, 50 μM; PPR = $97 \pm 8\%$ of control, $n = 4$, $P = 0.76$; **Fig. 1b**).

Reduced glutamate in cleft after PPD indicates MVR

Severe PPD is evident at cerebellar climbing fiber – Purkinje cell synapses, which exhibit very high release probability[6] as well as MVR[9]. MVR has been demonstrated at these synapses using a low-affinity glutamate receptor antagonist, the efficacy of which depends on the concentration of synaptic glutamate[9]. In paired-pulse experiments, the antagonist blocked the second EPSC more than the first[9], indicating that the glutamate in the cleft was reduced concomitantly with P_R, and MVR was more prevalent during the first EPSC. To assay MVR at a ribbon synapse, we examined the effects of a subsaturating concentration of kynurenic acid (KYN, 250 μM), a rapidly-dissociating AMPAR antagonist[23], on paired tEPSCs (25 ms interval; **Fig. 1c**). KYN blocked the second tEPSC more than the first ($70 \pm 4\%$ versus $42 \pm 4\%$ reduction, $n = 10$, $P = 0.01$; **Fig. 1c**), indicating a higher concentration of cleft glutamate during the first tEPSC.

For two reasons, the effects of KYN were unlikely to reflect voltage clamp errors. First, NBQX (100–300 nM), a high-affinity, slowly dissociating AMPAR antagonist whose efficacy is independent of cleft glutamate[23], blocked the second and first tEPSCs approximately equally ($56 \pm 7\%$ versus $50 \pm 7\%$ reduction, respectively, $n = 8$, $P = 0.06$; **Fig. 1d**). Second, paired tEPSCs recorded at different holding potentials exhibited similar depression (PPR at -45 mV was $110 \pm 3\%$ of that at -90 mV, $n = 13$, $P = 0.01$; **Fig. 1e**), even though halving the driving force on the underlying conductances reduced the amplitude of the first tEPSC by $51 \pm 1\%$. The effects of the aforementioned manipulations on PPR are summarized in **Figure 1f**.

tEPSC quantal content exceeds the number of synapses

The motor protein kinesin is found in synaptic ribbons[24]. In combination with PKC immunohistochemistry, which, in the retina, marks RBCs specifically[25], anti-kinesin antibodies have been used to label RBC synapses[26]. We estimated the number of synaptic contacts made by single RBCs using combined PKC and kinesin immunohistochemistry (**Fig. 2a**). Complete axonal arborization was reconstructed by tracing PKC-labeled axon terminals back to their somas of origin and counting kinesin-labeled puncta within the borders of the axon terminals. Each RBC contained 36 ± 5 (mean ± s.d., $n = 23$; **Fig. 2b**) ribbons. If, as in rabbit[27,28] and cat[29] retinae, each RBC contacts 3–5 AIIs, the average connection would comprise 7–12 ribbon synapses. Here, we will assume that there are ten contacts between a single RBC and a single AII.

We consider each ribbon to correspond to a single active zone, perhaps possessing multiple release sites but apposed to a single cluster of postsynaptic receptors on each of two postsynaptic processes[26]. Were MVR prevalent at these synapses, the number of quanta released during a tEPSC would exceed the number of synapses between an RBC and an AII. To test this possibility, we first calculated m by dividing the
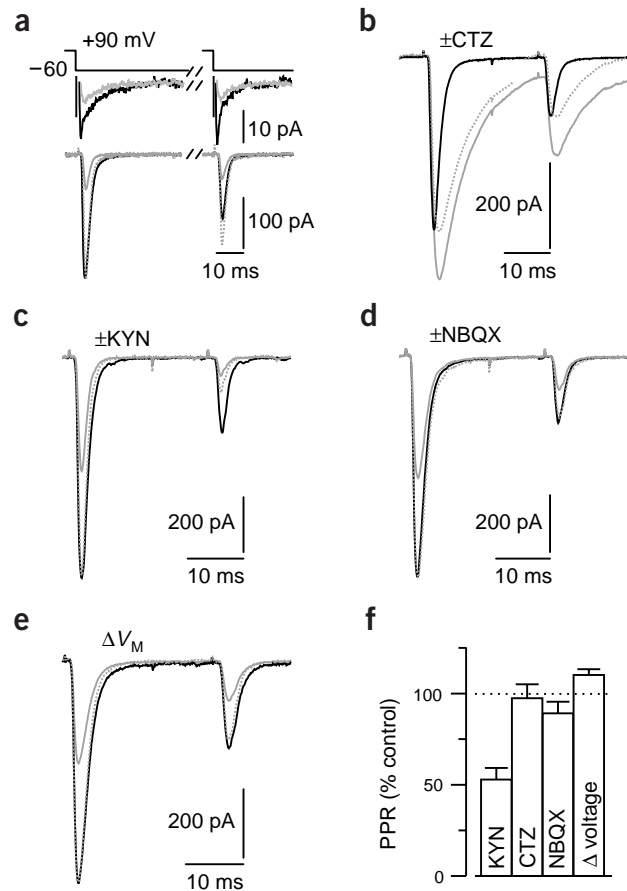

Figure 1 PPD of tEPSCs is presynaptic and reduces MVR. (**a**) tEPSCs (bottom traces) evoked by stepping the RBC to +90 mV for 10 ms (top traces) show PPD (100 ms interval) in 2.5 mM Ca^{2+} (black traces: PPR = 0.39 ± 0.05, $n = 6$). Presynaptic Ca^{2+} tail currents (middle traces) were not depressed. Lower traces: reducing external $[Ca^{2+}]$ to 0.5 mM (gray traces) reduced the tEPSC amplitude and the extent of PPD (PPR = 0.61 ± 0.04, $n = 6$). Low $[Ca^{2+}]$ traces scaled to control are shown as dashed lines; the same line color scheme applies to tEPSCs in **b**–**e**. (**b**) Blocking AMPAR desensitization with 50 μM CTZ had no effect on PPD (gray traces: dotted line is CTZ scaled to control, PPR = $97 \pm 8\%$ of control, $n = 4$). (**c**) The low-affinity AMPAR antagonist KYN (250 μM) blocked the second tEPSC more than the first and caused a profound reduction in the PPR ($53 \pm 6\%$ of control; $n = 10$). (**d**) The high-affinity antagonist NBQX (100 nM) inhibited the first and second tEPSC to a similar extent (PPR = $89 \pm 7\%$ of control). (**e**) Reducing the driving force by half reduced both tEPSCs by approximately half and had minimal effects on PPD (PPR = $110 \pm 3\%$ of control; $n = 13$). (**f**) Summary of the relative effects of the experimental manipulations of the first and second tEPSCs in **b**–**e**. Error bars are ± s.e.m.

charge transfer during the tEPSC (**Fig. 2c**) by that of the average mEPSC recorded in the same AII (**Fig. 2d**)[30]: $m = 39 \pm 3$ (range 3–124, $n = 64$; **Fig. 2b**). The tEPSC was nearly as fast as the mEPSC, although some slowing due to release asynchrony was apparent (tEPSC versus mEPSC: 10–90% rise time = 0.82 ± 0.02 versus 0.39 ± 0.01 ms; τ_{decay} = 1.84 ± 0.09 versus 0.90 ± 0.02 ms; $n = 64$). The release rate during the tEPSC, derived by deconvolving the mEPSC from the tEPSC[31–33], rose to a maximum of 23.2 ± 1.8 quanta/ms in 0.47 ± 0.01 ms and decayed with a time constant of 1.19 ± 0.05 ms ($n = 64$; **Fig. 2d**). Given the estimated number of contacts within the RBC-AII pairs (indeed, as the average m exceeds the average number of ribbons
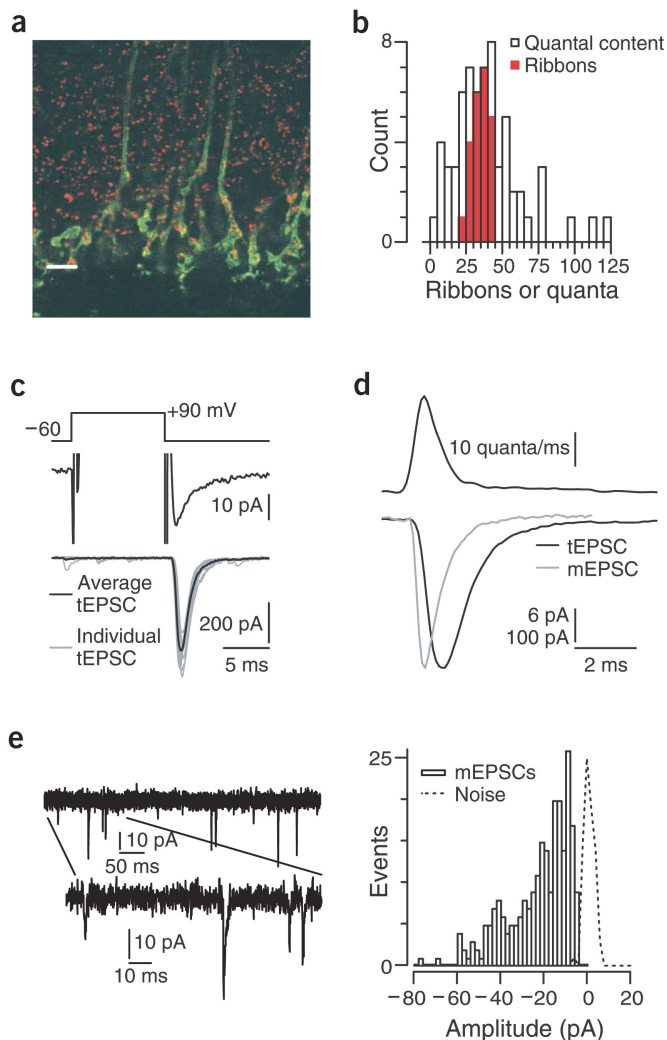
Figure 2 Quantal content of tEPSC exceeds the number of connections between an RBC-AII cell pair. (**a**) A single confocal section showing kinesin (red) and PKC (green) immunoreactivity in the inner part of the inner plexiform layer (scale bar, 5 μm). (**b**) Histogram showing distribution of the number of ribbons in 23 RBCs (measured by counting kinesin-positive spots) and the quantal content of recorded tEPSCs ($n = 64$). (**c**) An RBC was stepped to +90 mV for 10 ms (top trace), eliciting Ca^{2+} tail current (middle trace). Seven individual tEPSCs and the average tEPSC are shown (bottom). (**d**) The average mEPSC is deconvolved from the tEPSC (bottom traces) to yield an estimate of the instantaneous release rate (top trace). (**e**) Spontaneous mEPSCs (left) recorded in the same postsynaptic neuron were quite variable in amplitude and exhibit a skewed amplitude distribution (right).

within an RBC), it appears that single ribbon synapses release 4 vesicles/ms (39 vesicles/~10 contacts) to generate the tEPSC.

Miniature EPSCs are uniquantal

To calculate m, we assumed that, as at conventional synapses, spontaneous mEPSCs represent the postsynaptic responses to transmitter released from single vesicles. Though the size distribution of vesicles in mammalian RBC terminals has not been measured, two studies of goldfish Mb1 terminals report that those vesicle diameters are normally distributed around a mean (± s.d.) of 29 ± 4 nm (ref. 12) or 36 ± 6 nm (ref. 34). As small differences in diameter cause large changes in vesicle volume and transmitter content, a compact vesicle size distribution can generate a skewed and variable mEPSC

amplitude distribution, as we observed in our recordings[35] (**Fig. 2e**). Alternatively, some of the skew in this distribution could arise from a subpopulation of multiquantal events.

To determine whether mEPSCs at the RBC-AII synapse are uniquantal, we recorded mEPSCs as P_R was varied by altering external $[Ca^{2+}]$ (**Fig. 3**). Because MVR depends on P_R[7,9,10,18], the amplitude of multiquantal, but not quantal, events would be reduced by lowering P_R. Reducing the extracellular $[Ca^{2+}]$ from 2.5 mM to 0.5 mM increased the interval between mEPSCs (from 43 ± 13 ms to 101 ± 16 ms, $n = 12$, $P < 0.0001$; **Fig. 3a,b**) without changing the shape or mean of the amplitude distribution (amplitude $= 100 \pm 3\%$ of control, $n = 12$, $P = 0.79$; **Fig. 3c**). The metabotropic glutamate receptor agonist L-2-amino-4-phosphonobutyric acid (L-AP4, 2.5 μM), which reduces spontaneous release by hyperpolarizing ON bipolar cells[36], had similar effects (inter-event interval from 64 ± 8 ms to 217 ± 64 ms, $n = 6$, $P < 0.0001$; **Fig. 3d,e**; amplitude $= 100 \pm 3\%$ of control, $n = 6$, $P = 0.58$; **Fig. 3f**).

Although some mEPSCs could reflect MVR via an unknown mechanism that is insensitive to altered P_R, given their irreducibility, such events still can be considered quantal. In the absence of any evidence to the contrary, we will consider them to be univesicular.

Direct detection of coordinated MVR

The experiments above indicate that MVR occurs during tEPSCs at RBC synapses. Analogous results at synapses in the hippocampus[7,10] and cerebellum[8,9] suggest that MVR is a consequence of high P_R at active zones with multiple release sites. At inhibitory synapses in the cerebellum, individual quanta discerned within multivesicular events exhibited the same asynchrony inherent in the evoked EPSC[8], suggesting that individual release sites may contribute to MVR while remaining functionally independent.

At RBC synapses, the ribbon may provide a structural basis for coordinating release at multiple sites within an active zone[15]. To examine the activity of individual release sites, synaptic transmission was evoked in a manner such that release was desynchronized to an extent that individual synaptic events could be resolved. When presynaptic Ca^{2+} buffering capacity was reduced (0.2 mM EGTA in the presynaptic pipette), the EPSC exhibited a pronounced asynchronous component that persisted for hundreds of milliseconds following the termination of a presynaptic depolarizing step[19] (**Fig. 4a**). To reduce contamination by spontaneous activity at other excitatory synapses onto the AII, these experiments were performed in the presence of L-AP4 (**Fig. 3d–f**). Under these conditions, postsynaptic activity after the step was relatively low in the absence of asynchronous release (e.g., with 10 mM EGTA in the presynaptic pipette; **Fig. 4b**; also see ref. 19).

Individual asynchronous EPSCs (aEPSCs) occurring during the first 500 ms following the termination of the presynaptic voltage step (**Fig. 4a**, inset) were larger than spontaneous mEPSCs ($m = 1.50 \pm 0.15$; $P < 0.0001$ versus mEPSC), though their waveforms were similar (**Fig. 4c**; mEPSC versus aEPSC: 10–90% rise time $= 0.27 \pm 0.01$ versus 0.32 ± 0.01 ms; $\tau_{decay} = 0.89 \pm 0.03$ versus 0.93 ± 0.07 ms; $n = 4$). When P_R was lowered by reducing external $[Ca^{2+}]$ from 2.5 to 0.5 mM, m was reduced to 1.08 ± 0.09 ($P = 0.0082$ versus mEPSC; $P < 0.0001$ versus control) with little change in waveform: 10–90% rise time $= 95 \pm 1\%$ of control; $\tau_{decay} = 106 \pm 11\%$ of control (**Fig. 4c**; $n = 4$). The mEPSC amplitudes were unaffected by changing $[Ca^{2+}]$ (**Fig. 4c** and **Fig. 3a–c**). These results indicate that in normal $[Ca^{2+}]$, a substantial fraction of aEPSCs reflects MVR. The similarity in aEPSC and mEPSC rise time requires that individual quanta contributing to a multivesicular event be released nearly simultaneously (within 100 μs of each other). It is improbable that
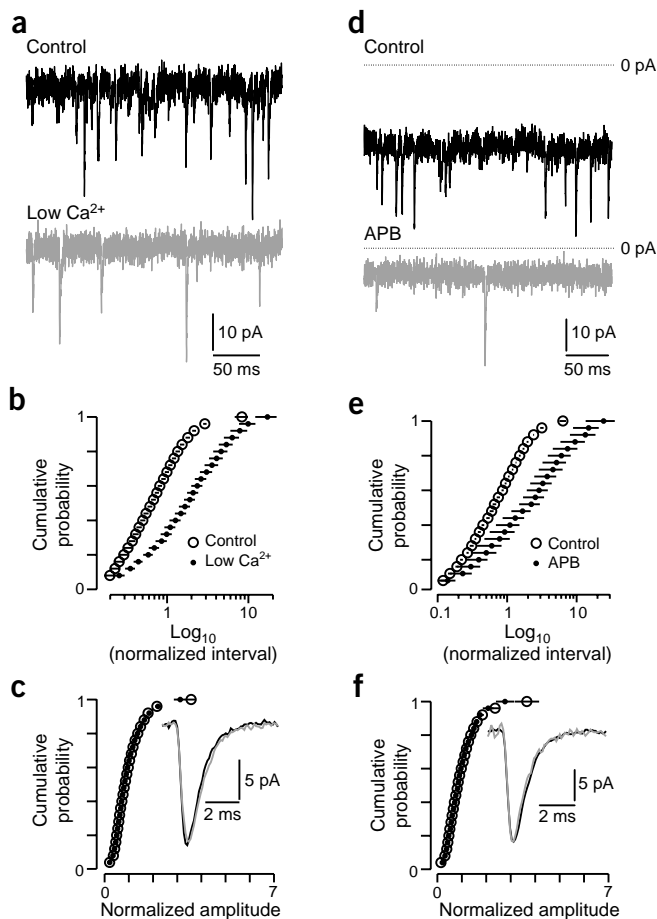
a

Control

Low Ca^{2+}

10 pA

50 ms

b

Cumulative probability

○ Control
● Low Ca^{2+}

1

10

Log$_{10}$
(normalized interval)

c

Cumulative probability

5 pA

2 ms

0   Normalized amplitude   7

d

Control

0 pA

APB

0 pA

10 pA

50 ms

e

Cumulative probability

○ Control
● APB

0.1   1   10

Log$_{10}$
(normalized interval)

f

Cumulative probability

5 pA

2 ms

0   Normalized amplitude   7

Figure 3 Spontaneous mEPSCs are uniquantal. (**a**) A continuous current recording (black trace, 500 ms) from an AII shows numerous spontaneous synaptic events, the frequency of which is reduced markedly when external [Ca^{2+}] is lowered (gray trace). (**b**) This reduction in mEPSC frequency (*i.e.*, an increase in interval) is summarized in a cumulative probability distribution (*n* = 12 cells). For each cell, inter-event intervals for control and low Ca^{2+} conditions were normalized to the mean control inter-event interval; individual distributions were then averaged. (**c**) The amplitude of the spontaneous events was unaffected by lowering [Ca^{2+}]. For each neuron, amplitudes for control and low Ca^{2+} events were normalized to the mean control amplitude (*n* = 12 cells; graph as in **b**). Inset: the average traces from one AII illustrate the fact that lowering [Ca^{2+}] did not affect the mEPSC amplitude or waveform (black, control; gray, low Ca^{2+}). (**d**) Spontaneous mEPSCs recorded in the absence (black) or presence (gray) of L-AP4 (2.5 µM). L-AP4 application caused a characteristic reduction in holding current (relative to the zero line above each trace). (**e**) The frequency of mEPSCs was reduced by L-AP4 (*n* = 6 cells). (**f**) The amplitude of spontaneous mEPSCs was unaffected by L-AP4; average traces are shown in the inset (*n* = 6 cells; graph as in **e**). Error bars in **b**,**c**,**e**,**f** are ± s.e.m.

fraction of the evoked responses arises from the coordinated exocytosis of multiple vesicles from a single active zone.

To confirm that the amplitude of the multiquantal evoked EPSCs was dependent on P_R, in some experiments the small presynaptic depolarization was preceded on alternate trials by a tEPSC (**Fig. 5a**, gray traces). In this paired-pulse paradigm, the tEPSC diminished the postsynaptic responses elicited by the step (**Fig. 5a**, average trace, and **Fig. 5b**). Although in some cases the mean amplitude of the individual depressed EPSCs was similar to that of the mEPSCs, on average they were slightly larger (*m* = 1.18 ± 0.08; *n* = 7; *P* = 0.008 versus mini; *P* < 0.0001 versus control; **Fig. 5b**), indicating that depression usually did not abolish MVR completely. Similar results were obtained in analogous experiments done at 35 °C (*n* = 3; **Fig. 5c**).

Coordinated MVR obeys binomial statistics

The synchrony of MVR observed here indicates that some mechanism at ribbon synapses—perhaps interactions within the ribbon itself—coordinates the simultaneous release of multiple vesicles. Does the ribbon mediate cooperative interactions between neighboring release sites during MVR, or does it simply synchronize sites or vesicles with independent release probabilities? If the latter is true,

this occurs randomly: given an aEPSC frequency of 100 Hz (**Fig. 4a**, inset), the chance of two events occurring within 100 µs is only one in 1,000. Consequently, the release of multiple quanta likely is synchronized at ribbon synapses.

Although the delayed (asynchronous) release process involves the same vesicles as exocytosis that occurs during Ca^{2+} influx[37], the multivesicular nature of the aEPSCs (**Fig. 4**) conceivably could reflect some peculiarity of asynchronous release. To determine whether coordinated MVR occurs under more physiological conditions, we evoked EPSCs using small presynaptic depolarizations (15–25 mV, 100 ms), comparable in magnitude to those recorded from RBCs following light stimulation[38]. The resultant postsynaptic responses were characterized by multiple small, distinct EPSCs occurring throughout the depolarization (**Fig. 5a**, black traces). Individual, desynchronized EPSCs were similar in time course to mEPSCs (inset, **Fig. 5b**; mEPSC versus EPSC: 10–90% rise time = 0.28 ± 0.01 versus 0.30 ± 0.01 ms; *P* = 0.003; τ$_{decay}$ = 0.78 ± 0.04 versus 0.80 ± 0.03 ms; *P* = 0.39; *n* = 12), but larger in amplitude (*m* = 1.58 ± 0.08, *n* = 12; *P* < 0.0001 versus mEPSCs; **Fig. 5b**). As with the aEPSCs described above, the similarity of the evoked and miniature EPSC rise times suggests that a
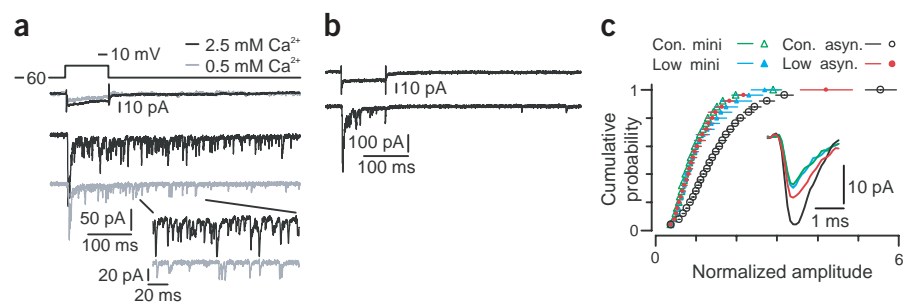
a

−10 mV
−60

── 2.5 mM Ca^{2+}
── 0.5 mM Ca^{2+}

10 pA

50 pA
100 ms

20 pA
20 ms

b

10 pA

100 pA
100 ms

c

Con. mini △ Con. asyn. ── ○
Low mini ▲ Low asyn. ── ●

Cumulative probability

10 pA

1 ms

0   Normalized amplitude   6

Figure 4 Analysis of asynchronous release reveals MVR. (**a**) With 0.2 mM EGTA in the presynaptic pipette, stepping the RBC to −10 mV evoked a compound EPSC followed by aEPSCs. Lowering external [Ca^{2+}] from 2.5 to 0.5 mM reduced the amplitude and frequency of the aEPSCs. (**b**) Currents evoked with 10 mM EGTA in the presynaptic pipette exhibited no asynchronous release and a low mEPSC frequency. (**c**) Normalized, cumulative probability distributions illustrate the fact that lowering P_R reduced aEPSC amplitude but not mEPSC amplitude (key above graph: control mEPSCs, green triangles; mEPSCs in low Ca^{2+}, blue triangles; control aEPSCs, black circles; aEPSCs in low Ca^{2+}, red circles; *n* = 4 RBC-AII pairs). Representative average waveforms for each condition (colors as above) are shown in the inset. Error bars are ± s.e.m.

Figure 5 MVR is observed when release is desynchronized. (**a**) Presynaptic voltage steps to –45 mV (100 ms) elicited small Ca^{2+} currents (top traces) and EPSCs (below). In alternate trials (six of which are illustrated), the 100-ms Ca^{2+} current was preceded by a Ca^{2+} tail current (gray traces) resulting in depression of the average ensemble EPSC (at bottom). (**b**) Normalized cumulative probability distributions for seven experiments illustrate that synaptic depression reduces the amplitude of the evoked EPSCs (average postsynaptic currents in inset). (**c**) The same experiment as in **a** and **b** repeated at 35 °C ($n = 3$). Error bars in **b** and **c** are ± s.e.m.
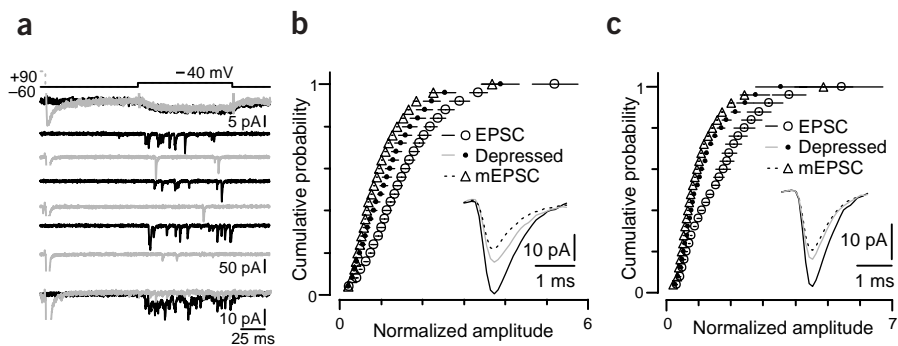
then it should be possible to predict the amplitude distribution of the evoked EPSCs from the mEPSC distribution: quantal events would combine randomly according to binomial statistics to generate individual multivesicular EPSCs[30]. In the simplest case, binomial statistics would describe MVR if n individual release sites were independent and equal in regard to their release probability p; cooperative interactions between release sites would violate the requirement of independence and cause a deviation from a binomial prediction.

EPSC distributions (**Fig. 6a,b**) were constructed by pooling all recorded asynchronous (**Fig. 4**) or small desynchronized (**Fig. 5**) EPSCs and normalizing all events from each experiment to the mean mEPSC amplitude from that experiment, such that the mean amplitude of the mEPSC distribution was 1 and the average value of the histogram was m. We simulated EPSC distributions by using a Monte Carlo approach to combine these mEPSCs at random and calculated the quantal parameters, n and p, that could give rise to the distribution (Methods).

The predicted EPSC distribution matched most closely the experimental distribution when $n = 2$ and $p = 0.78$ (**Fig. 6a**; see Methods for why $m \neq np$). The amplitude distributions of multiquantal aEPSCs also were described best when $n = 2$ ($p = 0.74$; **Fig. 6b**). An initial peak in the predicted asynchronous EPSC histogram that was not observed in the experimental data arose from the jagged mEPSC amplitude distribution, which comprised a relatively small number of events in these experiments. This discrepancy added significantly to the error between the asynchronous event distribution and the binomial prediction for all values of n (**Fig. 6b**, inset).

If PPD is due to depletion of releasable vesicles, PPD should cause a decrease in p, and the amplitude distribution of the desynchronized evoked events following a tEPSC should be described by binomial statistics when $n = 2$ and p corresponds to the reduced value of m. Consistent with this prediction, the depressed amplitude distribution was described well by binomial statistics when $n = 2$ and $p = 0.37$ (**Fig. 6a**). This predicted decrease in p corresponded well to the PPD observed experimentally with tEPSCs (**Figs. 1** and **6c**). Similarly, the aEPSCs recorded in low $[Ca^{2+}]$ were described well by binomial statistics when $n = 2$ and $p = 0.21$ (**Fig. 6b**), and the inferred effect on p corresponded well to the effects on the tEPSC amplitude of changing $[Ca^{2+}]$ (**Fig. 6c**).

Lowering $[Ca^{2+}]$ (**Fig. 4a**) or inducing depression (**Fig. 5a**) reduced the frequency of evoked desynchronized events. Binomial statistics cannot predict absolute event frequency, but predicted changes in frequency can be inferred from changes in the probability of seeing an event (i.e., $1 - p_0$). The ratio of $1 - p_0$ predicted by binomial statistics made a reasonable approximation of the experimentally observed changes in event frequency (**Fig. 6d**). Thus, simple binomial statistics predicted the amplitude distribution and frequency of evoked,

desynchronized events and the effects of changing release probability on large tEPSCs, suggesting both that MVR involves the temporal synchronization of otherwise independent release events and that binomial statistics govern release from the ribbon as a whole.

DISCUSSION

Exocytosis from multiple release sites in the same active zone

MVR observed at other central synapses[7–10] exhibits the same temporal jitter inherent in evoked release overall[8], suggesting that MVR reflects the asynchronous action of multiple, independent release sites within a presynaptic active zone. In contrast, our results indicate that multiple vesicles at ribbon synapses can fuse practically simultaneously, even when overall release is desynchronized. The quantal components within individual multivesicular events arise within 100 µs of each other (**Figs. 4** and **5**) and are much more synchronized than the release underlying even the fastest tEPSCs (**Fig. 2c**). We conclude that coordinated vesicle fusion at multiple release sites occurs at ribbon synapses and, therefore, that these synapses constitute an exception to the traditional notion that release sites within an active zone operate independently.

MVR reflects coordination but not cooperation

Evoked tEPSCs at RBC synapses reflect high P_R: paired tEPSCs exhibited pronounced PPD (PPR = 0.4). The differential block of the first and second responses by KYN indicates that MVR occurs during a tEPSC (**Fig. 1**), and consistent with this, the tEPSC $m = 39 \pm 3$, exceeding the number of contacts (~10) between a RBC-AII pairs (**Fig. 2**). We estimated that a single ribbon can release ~4 vesicles within 1 ms (**Fig. 2d**). Importantly, the postsynaptic AMPARs do not appear to be saturated by synaptically released glutamate (CTZ, which increases AMPAR affinity for glutamate, potentiates mEPSCs and large, evoked EPSCs similarly[19]) and therefore can encode MVR.

MVR also occurs when release is very desynchronized, as during asynchronous release (**Fig. 4**) and small depolarizing presynaptic steps (**Fig. 5**). Because the average amplitude of these small evoked events was sensitive to changes in P_R, unlike that of quantal mEPSCs, we conclude that they are multivesicular. Because the similarity of the mEPSC and evoked EPSC rise times requires that the individual vesicles within a multivesicular event be released with much greater synchrony than achieved during even the fastest tEPSCs (e.g., **Fig. 2d**), the MVR observed in these desynchronized events likely reflects coordination among multiple release sites.

The coefficient of variation (s.d./mean) of the mEPSC distribution is so large (~0.6) that quantal peaks in EPSC distributions are not evident (**Fig. 6**). EPSC distributions, however, were predicted well by scaling the mEPSC amplitudes according to simple binomial statistics (**Fig. 6**).
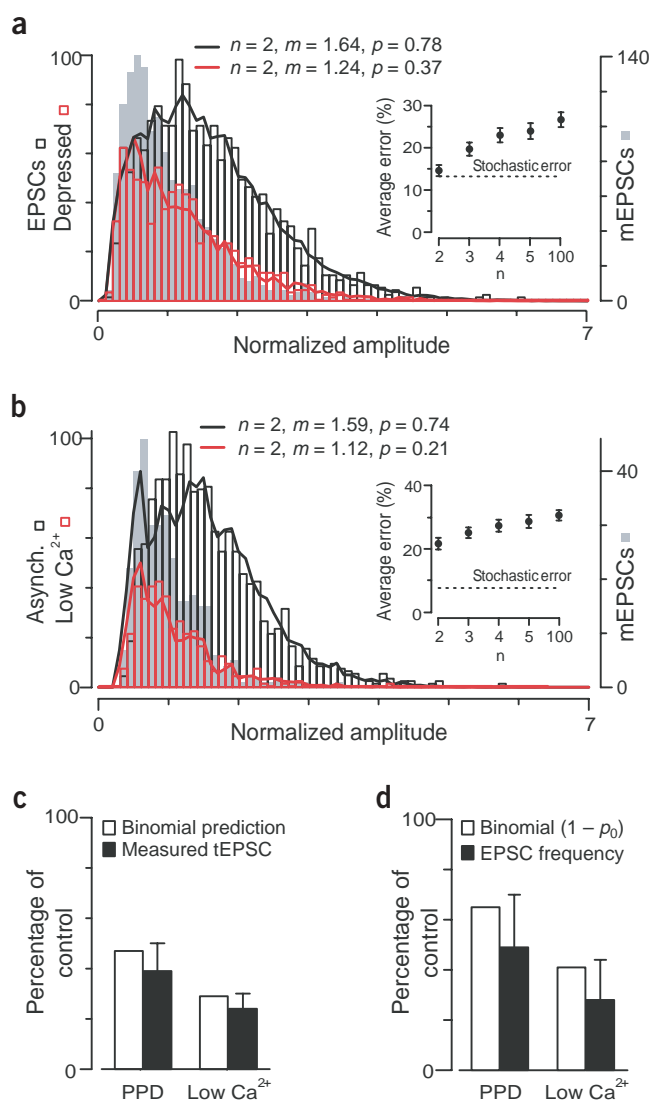
Figure 6 MVR obeys binomial statistics. (**a**) Normalized amplitude distributions for mEPSCs (solid gray bars), small evoked EPSCs (black bars) and depressed EPSCs (red bars) pooled from seven experiments. The solid lines are the distributions predicted by binomial statistics when $n = 2$. Inset: a comparison of the error (mean ± s.d.) between the binomial prediction and the evoked distribution for different values of n (see Methods). (**b**) Normalized amplitude distributions for mEPSCs (solid gray bars), aEPSCs (black bars) and aEPSCs in low $[Ca^{2+}]$ (red bars) pooled from four experiments. The solid lines are the distributions predicted by binomial statistics when $n = 2$. Inset as in **a**. (**c**) The open bars are the ratios of the predicted p in control conditions to p when P_R was lowered by PPD or low external $[Ca^{2+}]$ for evoked and asynchronous EPSCs, respectively (binomial predictions in **a** and **b**). The black bars show the average tEPSC PPR and the average change in tEPSC amplitude in low external $[Ca^{2+}]$ (*e.g.*, **Fig. 1a**; $n = 6$). (**d**) The open bars are the ratios of the predicted probability of an event $(1 - p_0$ from the binomial prediction) under control and low P_R conditions (PPD or low $[Ca^{2+}]$; **a** and **b**, respectively). The black bars show the changes in desynchronized EPSC frequency that occurred during PPD (data in **a**; $n = 7$) or in low $[Ca^{2+}]$ (data in **b**; $n = 4$). The error bars are ± s.d.

is, within a single active zone. Based on the anatomy of the ribbon (vesicles on either side of a central plane; see ref. 12), it is possible that two sites—perhaps located on opposite sides of the ribbon—form a 'release-site pair.' Release could be synchronized within this pair if the two sites sensed a common, short-lived microdomain of Ca^{2+} influx. This seems an unlikely explanation for our results, however, because coordinated MVR is observed during asynchronous release (**Fig. 4**), which occurs well after the closure of Ca^{2+} channels and, presumably, the collapse of any Ca^{2+} microdomains. Alternatively, it is possible that release within a pair is synchronized by the ribbon itself and that release-site pairs distributed along the ribbon are activated with the asynchrony inherent in the tEPSC while release within each pair is highly synchronized.

The mechanisms underlying coordinated MVR are uncertain, but, very generally, the simultaneous release of more than one vesicle's contents could be accomplished in two ways. First, multiple vesicles could fuse simultaneously with the presynaptic membrane ('coincident fusion'). Second, two or more vesicles within the terminal could incorporate into a single, larger vesicle prior to exocytosis, analogous to the "compound fusion" that occurs during secretion from mast cells[41]. Although it has not been observed directly in neurons, a recent review[15] suggests that the synaptic ribbon may provide a site at which compound fusion can occur prior to exocytosis.

Our observations can be explained by either coincident or compound fusion. In the case of coincident fusion, the prevalence of coordinated MVR would reflect the release probability of the individual sites within a release-site pair (**Fig. 6**). Compound fusion would depend on P_R if the ability of vesicles to fuse to each other were regulated in a Ca^{2+}-dependent manner, just as their ability to fuse with the plasma membrane is regulated. This is not unlikely, as the fusion of two vesicles involves the same interactions of v/SNARE and t/SNARE proteins, as does the fusion of vesicles and the plasma membrane[15,42]. Large vesicles created by compound fusion, however, would contain more v/SNARE and t/SNARE proteins than single vesicles, and therefore would be more likely to fuse with other vesicles than with the plasma membrane. This would result in a form of cooperativity that would generate a disproportionate number of relatively large synaptic events, thereby violating the assumptions inherent in the application of binomial statistics. Our experimental results, taken together with the fact that the EPSC distributions appear to reflect a binomial process, therefore are more consistent with the coincident fusion model.

Additionally, the change in the EPSC amplitude distributions caused by reducing the external $[Ca^{2+}]$ or by inducing synaptic depression was accounted for simply by reducing p so that the predicted m matched that obtained experimentally. These results suggest that vesicles released within distinct multivesicular events, though nearly perfectly synchronized, do not interact cooperatively. Binomial statistics also provided a reasonable approximation of the experimental change in tEPSC amplitude induced by depression or changing $[Ca^{2+}]$ (**Fig. 6c**), as well as the decrease in event frequency under conditions favoring desynchronized release (**Fig. 6d**). The modest, though consistent, underestimation of the experimental effects of changing p does suggest, however, either that p may be higher during a tEPSC, or that other processes may play minor roles in determining P_R during a tEPSC.

Coordinated MVR: a role for the ribbon?

Although ectopic release at sites separate from active zones occurs at both climbing fiber synapses[39] and isolated goldfish Mb1 terminals[40], we believe that the release synchrony and fast receptor activation reflected in the rapidly rising multivesicular events reported here requires that the contents of two vesicles be released in close proximity to each other and to the same postsynaptic receptors, that

MVR and mEPSC frequency are [Ca^{2+}]-dependent, but mEPSC amplitude is not (**Figs. 3** and **4**), suggesting that MVR requires a degree of Ca^{2+} influx that occurs only during an evoked response. It is possible, however, that mEPSCs reflect sub-quantal release of neurotransmitter (*i.e.*, incomplete or partial fusion, also known as "kiss-and-run" release[43]), and that evoked EPSCs reflect single, complete exocytotic events triggered by Ca^{2+} influx through a number of open Ca^{2+} channels rather than MVR at each synapse. In this scenario, the reduction in EPSC amplitude during short-term depression would be achieved by a Ca^{2+}-dependent transition from full to partial vesicle fusion. Were this true, however, significant discrepancies between the binomial predictions and measured EPSC amplitude distributions would arise because mEPSCs would not be quantal. In light of the good agreement between evoked EPSC amplitudes and binomial statistics (**Fig. 6**) and the fact that ribbons appear designed to deliver multiple vesicles to the presynaptic membrane rather than prevent their complete fusion, we favor the interpretation that EPSCs at RBC-AII synapses are generated by MVR, and that a reduction in MVR underlies synaptic depression.

Implications for scotopic signal processing

The AII amacrine cell is a critical component of the mammalian rod circuit, which transfers rod photoreceptor responses to ganglion cells, the output cells of the retina, at low (scotopic) light intensities. The rod pathway seems to be optimized to process very small signals, as ganglion cells can respond to the absorption of a single photon[44,45]. To accomplish this, however, the circuit must overcome a problem imposed by the substantial convergence of rods onto AIIs through RBCs[27–29]: how can minute, light-induced changes in rod membrane potential be differentiated from photoreceptor noise at the level of the RBC, and, once this is accomplished, how can the signal be preserved as it is passed across synapses? Near its threshold, the AII light response is non-linear[46]. Recently, signal transfer from mammalian rods to RBCs was found to be non-linear as well, indicating that fluctuations in RBC responses were greater than expected from simple summation of rod inputs[47]. It was suggested that it could be advantageous for this threshold-like non-linearity to be repeated at the RBC-AII synapse to prevent AIIs from summing the noise generated in the presynaptic bipolar cells[47]. Coordinated MVR is a simple mechanism by which this can be achieved: if evoked EPSCs are always larger than spontaneous mEPSCs (*e.g.*, **Fig. 5**), the postsynaptic neuron is provided with a way to distinguish light-evoked signals from synaptic noise. If the synapse does operate in this manner, severely depressed inputs may not exert discernable postsynaptic effects; in discarding small signals, the synapse would sacrifice sensitivity for accuracy, as occurs at rod-RBC synapses[47].

METHODS

Review of experimental design. All procedures were done in accordance with the guidelines of University of Pennsylvania and the National Institutes of Health.

Electrophysiology. Experiments were done at ~22 °C (except where indicated) in light-adapted retinal slices (200 μm thick) taken from Sprague-Dawley rats (P15–25), as described previously[19]. In most cases, slices were taken from the mid-temporal retina. Retinae were isolated in artificial cerebrospinal fluid (ACSF) containing 119 mM NaCl, 23 mM NaHCO₃, 10 mM glucose, 1.25 mM NaH₂PO₄, 2.5 mM KCl, 2.5 mM CaCl₂, 1.5 mM MgSO₄, 2 mM sodium lactate and 2 mM sodium pyruvate, and embedded in low–melting point agarose (4% in ACSF without glucose, sodium lactate and sodium pyruvate, and with 4-(2-hydroxyethyl)-1-piperazineethanesulfonic acid (HEPES) substituted for NaHCO₃).

Whole-cell voltage-clamp recordings were made from AII amacrine cells and RBCs in the presence of picrotoxin (100 μM), TPMPA (50 μM), strychnine (0.5 μM) and TTX (0.25 μM) to block GABA$_A$ receptor–, GABA$_C$ receptor–, glycine receptor– and voltage-gated Na^+ channel–mediated currents, respectively. For AII recordings, holding potential (V_M) was –60 or –90 mV and pipettes (~5 MΩ) contained 90 mM CsCH₃SO₃, 20 mM tetraethylammonium chloride (TEA-Cl), 10 mM HEPES, 10 mM ethylene glycol bis(2-aminoethyl ether)-*N,N,N′,N′*-tetraacetic acid (EGTA), 10 mM sodium phosphocreatine, 4 mM adenosine triphosphate in the form MgATP and 0.4 mM guanosine triphosphate in the form NaGTP (junction potential ≈ 10 mV; indicated V_M corrected accordingly). For recording from RBCs (V_M = –60 mV), pipettes (~10 MΩ) were filled with 90 mM CsCH₃SO₃, 20 mM TEA-Cl, 10 mM HEPES, 10 mM glutamic acid, 10 mM sodium phosphocreatine, 1.5 mM *O,O′*-bis(2-aminophenyl)ethylene glycol-*N,N,N′,N′*-tetraacetic acid (BAPTA), 4 mM MgATP and 0.4 mM NaGTP. In some cases, fluorescent tracers (Alexa hydrazines, Molecular Probes) were included in the pipettes, which were coated with dental wax to reduce their capacitance. Postsynaptic access resistance (R_{access}) was <20 MΩ, compensated 70–90%; presynaptic R_{access} was 25–50 MΩ and not compensated. All drugs and chemicals were obtained from Sigma or Tocris (except for TTX, from Alamone Labs); drugs were prepared as concentrated (at least 1,000×) stock solutions and diluted into the ACSF prior to the experiments.

EPSCs were evoked at 17-s intervals and recorded using two Axopatch 200B amplifiers or one MultiClamp 700A amplifier (Axon Instruments). Currents were low-pass filtered at 2 kHz and digitized at 10 kHz by an Instrutech ITC-18 A/D board controlled by software written for Igor Pro (WaveMetrics). Amplifier command potentials were generated on the Instrutech board; a P/4 leak-subtraction protocol was used to reveal the presynaptic calcium ion current (I_{Ca}). Data analysis was done using Igor Pro and Excel (Microsoft). Spontaneous, mEPSCs were detected based on the first derivative of the current rising phase, and all detected events were inspected by eye.

Tissue fixation and immunohistochemistry. Adult rats under deep sodium pentobarbital anesthesia (50 mg/kg) were enucleated and then killed by a pentobarbital overdose. The posterior half of the eye was fixed at ~22 °C by immersion in buffered 4% paraformaldehyde (10 min). Following rinse and overnight cryoprotection in 0.1M phosphate buffer containing 30% sucrose, the central area was embedded in 4% agarose and sectioned radially with a vibratome (Vibratome Company). Sections (200 μm thick) were pre-incubated in diluent containing 10% normal goat serum, 5% sucrose, 0.01% sodium azide and 0.5% Triton X-100 in 0.1M phosphate buffer for 1 h at ~22 °C, incubated in antibody to PKC (anti-PKC) overnight at 4 °C, washed and incubated in anti-mouse-Cy3 (F(ab′) fragments), and then incubated in antibody to kinesin (anti-kinesin) followed by anti-mouse–Alexa 488 (IgG). Control experiments in which the second primary antibody was omitted indicated that the second secondary did not react with the anti-PKC. The monoclonal anti-PKC (clone MC5) was from Sigma and monoclonal anti-kinesin (clone K2.4) was from Covance Inc. Stacks of 32 optical confocal sections (×100, NA 1.4, zoom 2, 0.5 μm z-step) were analyzed with OpenLab software (Improvision). PKC-stained cells were reconstructed manually and the kinesin spots counted in each cell. Typically, ribbons in rod bipolar cells are large. A fluorescent spot was counted as a ribbon if its diameter was greater than 0.25 μm; the spots had an average diameter of 0.5 μm. This is likely larger than the actual size of the ribbons, owing to the fluorescent 'halo' emanating from the signal. The average intensity of the faintest spot was five times greater than background, and spots with a smaller signal-to-noise ratio were not encountered.

Monte Carlo simulations of EPSC amplitude distributions. Estimations of the desynchronized, evoked EPSC amplitude distributions were constructed using the mEPSC amplitudes and a Monte Carlo algorithm that obeyed simple binomial statistics (Igor Pro, illustrated in **Fig. 6**). According to the binomial equation, when failures of transmission are included in the calculation of quantal content, $m = np$ (ref. 30). When failures are excluded (failures were undetectable in our experiments because release was desynchronized; **Figs. 4** and **5**), m exceeds np by a factor equal to $1/(1 - p_0)$, where $p_0 = (1 - p)^n$. In either case, the experimental data permits only one free parameter, because for a given value of n there is a unique p that yields the experimentally measured quantal content m.

We chose an integral n and generated an initial estimate of p from the experimentally measured m, as above. For each of N events in the measured evoked distribution, n random numbers between 0 and 1 were generated, and for each value less than p, quantal amplitude(s) were chosen at random from the mEPSC amplitude distribution and summed to yield an EPSC amplitude. The relative number of 'singles,' 'doubles,' and so on generated randomly by this process nicely matched the numbers predicted by the binomial equation after adjusting for the lack of failures (see above). A histogram of N simulated EPSC amplitudes was constructed, the average value of which was m. This entire process was repeated 20 times to produce the average predicted histograms illustrated in **Figure 6**. The error between predicted and experimental histograms was determined by calculating the average difference between corresponding bins of each of the 20 the predicted histograms and a smoothed copy of the experimental histogram as a percentage of the number of events in each bin of the experimental histogram (*e.g.*, **Fig. 6A**, inset). 'Stochastic error,' which results from sampling a finite number of events from a noisy distribution, was estimated by calculating the average of the differences between each bin of the experimental histogram and a smoothed copy.

Statistics. Differences in amplitude and inter-event interval distributions were assayed for significance by the Mann-Whitney *U*-test; differences in actual and predicted EPSC amplitude distributions were tested by the Kolmogorov-Smirnov test; otherwise, paired, two-tailed *t*-tests were used to compare the data sets. Significance was accepted as $P < 0.05$. Unless stated otherwise, all data are presented as mean ± standard error (s.e.m.), and illustrated traces are averages of 5–10 responses.

COMPETING INTERESTS STATEMENT
The authors declare that they have no competing financial interests.

1. Propst, J.W. & Ko, C.P. Correlations between active zone ultrastructure and synaptic function studied with freeze-fracture of physiologically identified neuromuscular junctions. *J. Neurosci.* **7**, 3654–3664 (1987).
2. Katz, B. *The Release of Neural Transmitter Substances* (Liverpool University Press, Liverpool, UK, 1969).
3. Redman, S. Quantal analysis of synaptic potentials in neurons of the central nervous system. *Physiol. Rev.* **70**, 165–198 (1990).
4. Korn, H. & Faber, D.S. Quantal analysis and synaptic efficacy in the CNS. *Trends Neurosci.* **14**, 439–445 (1991).
5. Stevens, C.F. & Wang, Y. Facilitation and depression at single central synapses. *Neuron* **14**, 795–802 (1995).
6. Silver, R.A., Momiyama, A. & Cull-Candy, S.G. Locus of frequency-dependent depression identified with multiple-probability fluctuation analysis at rat climbing fibre-Purkinje cell synapses. *J. Physiol.* **510**, 881–902 (1998).
7. Tong, G. & Jahr, C.E. Multivesicular release from excitatory synapses of cultured hippocampal neurons. *Neuron* **12**, 51–59 (1994).
8. Auger, C., Kondo, S. & Marty, A. Multivesicular release at single functional synaptic sites in cerebellar stellate and basket cells. *J. Neurosci.* **18**, 4532–4547 (1998).
9. Wadiche, J.I. & Jahr, C.E. Multivesicular release at climbing fiber-Purkinje cell synapses. *Neuron* **32**, 301–313 (2001).
10. Oertner, T.G., Sabatini, B.L., Nimchinsky, E.A. & Svoboda, K. Facilitation at single synapses probed with optical quantal analysis. *Nat. Neurosci.* **5**, 657–664 (2002).
11. Silver, R.A., Lubke, J., Sakmann, B. & Feldmeyer, D. High-probability uniquantal transmission at excitatory synapses in barrel cortex. *Science* **302**, 1981–1984 (2003).
12. von Gersdorff, H., Vardi, E., Matthews, G. & Sterling, P. Evidence that vesicles on the synaptic ribbon of retinal bipolar neurons can be rapidly released. *Neuron* **16**, 1221–1227 (1996).
13. Heidelberger, R., Heinemann, C., Neher, E. & Matthews, G. Calcium dependence of the rate of exocytosis in a synaptic terminal. *Nature* **371**, 513–515 (1994).
14. von Gersdorff, H. & Matthews, G. Depletion and replenishment of vesicle pools at a ribbon-type synaptic terminal. *J. Neurosci.* **17**, 1919–1927 (1997).
15. Parsons, T.D. & Sterling, P. Synaptic ribbon: conveyor belt or safety belt. *Neuron* **37**, 379–382 (2003).
16. Strettoi, E., Dacheux, R.F. & Raviola, E. Synaptic connections of rod bipolar cells in the inner plexiform layer of the rabbit retina. *J. Comp. Neurol.* **295**, 449–466 (1990).
17. Chun, M.H., Han, S.H., Chung, J.W. & Wassle, H. Electron microscopic analysis of the rod pathway of the rat retina. *J. Comp. Neurol.* **332**, 421–432 (1993).
18. Tong, G. & Jahr, C.E. Block of glutamate transporters potentiates postsynaptic excitation. *Neuron* **13**, 1195–1203 (1994).
19. Singer, J.H. & Diamond, J.S. Sustained Ca^{2+} entry elicits transient postsynaptic currents at a retinal ribbon synapse. *J. Neurosci.* **23**, 10923–10933 (2003).
20. Cui, J., Ma, Y.P., Lipton, S.A. & Pan, Z.H. Glycine receptors and glycinergic synaptic input at the axon terminals of mammalian retinal rod bipolar cells. *J. Physiol.* **553**, 895–909 (2003).
21. Hartveit, E. Reciprocal synaptic interactions between rod bipolar cells and amacrine cells in the rat retina. *J. Neurophysiol.* **81**, 2923–2936 (1999).
22. Koulen, P. *et al.* Presynaptic and postsynaptic localization of $GABA_B$ receptors in neurons of the rat retina. *Eur. J. Neurosci.* **10**, 1446–1456 (1998).
23. Diamond, J.S. & Jahr, C.E. Transporters buffer synaptically released glutamate on a submillisecond time scale. *J. Neurosci.* **17**, 4672–4687 (1997).
24. Muresan, V., Lyass, A. & Schnapp, B.J. The kinesin motor KIF3A is a component of the presynaptic ribbon in vertebrate photoreceptors. *J. Neurosci.* **19**, 1027–1037 (1999).
25. Young, H.M. & Vaney, D.I. Rod-signal interneurons in the rabbit retina: 1. rod bipolar cells. *J. Comp. Neurol.* **310**, 139–153 (1991).
26. Li, W., Trexler, E.B. & Massey, S.C. Glutamate receptors at rod bipolar ribbon synapses in the rabbit retina. *J. Comp. Neurol.* **448**, 230–248 (2002).
27. Strettoi, E., Raviola, E. & Dacheux, R.F. Synaptic connections of the narrow-field, bistratified rod amacrine cell (AII) in the rabbit retina. *J. Comp. Neurol.* **325**, 152–168 (1992).
28. Vaney, D.I., Gynther, I.C. & Young, H.M. Rod-signal interneurons in the rabbit retina: 2. AII amacrine cells. *J. Comp. Neurol.* **310**, 154–169 (1991).
29. Sterling, P., Freed, M.A. & Smith, R.G. Architecture of rod and cone circuits to the on-beta ganglion cell. *J. Neurosci.* **8**, 623–642 (1988).
30. del Castillo, J. & Katz, B. Quantal components of the end-plate potential. *J. Physiol.* **124**, 157–181 (1954).
31. Van der Kloot, W. Estimating the timing of quantal releases during end-plate currents at the frog neuromuscular junction. *J. Physiol.* **402**, 595–603 (1988).
32. Diamond, J.S. & Jahr, C.E. Asynchronous release of synaptic vesicles determines the time course of the AMPA receptor-mediated EPSC. *Neuron* **15**, 1097–1107 (1995).
33. Isaacson, J.S. & Walmsley, B. Counting quanta: direct measurements of transmitter release at a central synapse. *Neuron* **15**, 875–884 (1995).
34. Lagnado, L., Gomis, A. & Job, C. Continuous vesicle cycling in the synaptic terminal of retinal bipolar cells. *Neuron* **17**, 957–967 (1996).
35. Frerking, M., Borges, S. & Wilson, M. Variation in GABA mini amplitude is the consequence of variation in transmitter concentration. *Neuron* **15**, 885–895 (1995).
36. Slaughter, M.M. & Miller, R.F. 2-amino-4-phosphonobutyric acid: a new pharmacological tool for retina research. *Science* **211**, 182–185 (1981).
37. Otsu, Y. *et al.* Competition between phasic and asynchronous release for recovered synaptic vesicles at developing hippocampal autaptic synapses. *J. Neurosci.* **24**, 420–433 (2004).
38. Euler, T. & Masland, R.H. Light-evoked responses of bipolar cells in a mammalian retina. *J. Neurophysiol.* **83**, 1817–1829 (2000).
39. Matsui, K. & Jahr, C.E. Ectopic release of synaptic vesicles. *Neuron* **40**, 1173–1183 (2003).
40. Zenisek, D., Steyer, J.A. & Almers, W. Transport, capture and exocytosis of single synaptic vesicles at active zones. *Nature* **406**, 849–854 (2000).
41. Alvarez deToledo, G. & Fernandez, J.M. Compound versus multigranular exocytosis in peritoneal mast cells. *J. Gen. Physiol.* **95**, 397–409 (1990).
42. Hansen, N.J., Antonin, W. & Edwardson, J.M. Identification of SNAREs involved in regulated exocytosis in the pancreatic acinar cell. *J. Biol. Chem.* **274**, 22871–22876 (1999).
43. Alvarez deToledo, G., Fernandez-Chacon, R. & Fernandez, J.M. Release of secretory products during transient vesicle fusion. *Nature* **363**, 554–558 (1993).
44. Barlow, H.B., Levick, W.R. & Yoon, M. Responses to single quanta of light in retinal ganglion cells of the cat. *Vision Res.* **3** (Suppl.), 87–101 (1971).
45. Sakitt, B. Counting every quantum. *J. Physiol.* **223**, 131–150 (1972).
46. Nelson, R. AII amacrine cells quicken time course of rod signals in the cat retina. *J. Neurophysiol.* **47**, 928–947 (1982).
47. Field, G.D. & Rieke, F. Nonlinear signal transfer from mouse rods to bipolar cells and implications for visual sensitivity. *Neuron* **34**, 773–785 (2002).